Bioorganic & Medicinal Chemistry 19 (2011) 6608–6614

Contents lists available at ScienceDirect

Bioorganic & Medicinal Chemistry

journal homepage: www.elsevier.com/locate/bmc

Palmerolide macrolides from the Antarctic tunicate *Synoicum adareanum*

Jaime H. Noguez [a], Thushara K. K. Diyabalanage [a], Yoshinari Miyata [a], Xiao-Song Xie [b], Frederick A. Valeriote [c], Charles D. Amsler [d], James B. McClintock [d], Bill J. Baker [a,*]

[a] Department of Chemistry and Center for Molecular Diversity in Drug Design, Discovery, and Delivery, University of South Florida, 4202 East Fowler Avenue, Tampa, FL 33620, USA
[b] McDermott Center for Human Growth and Development, UT Southwestern Medical Center, 5323 Harry Hines Blvd, Dallas, TX 75390, USA
[c] Henry Ford Health System, Josephine Ford Cancer Center, 1 Ford Place, Detroit, MI 48202, USA
[d] Department of Biology, University of Alabama at Birmingham, Birmingham, AL 35294, USA

ARTICLE INFO

Article history:
Available online 16 June 2011

Keywords:
Melanoma
V-ATPase inhibitor
Polyketide

ABSTRACT

Palmerolides D–G are new bioactive macrolides isolated from the Antarctic tunicate *Synoicum adareanum* and are related to the melanoma-selective cytotoxin palmerolide A. Most of these palmerolides are potent V-ATPase inhibitors and have sub-micromolar activity against melanoma. Though palmerolide A remains the most potent of this series of natural products against mammalian V-ATPase, recent data suggests that palmerolide D is the most potent against melanoma. A comparison of the bioactivity data obtained for these natural product palmerolides has provided insight into the substructures necessary to retain V-ATPase inhibition and cytotoxic activity.

1. Introduction

The ubiquitous trans-membrane vacuolar ATPases regulate cellular and organellular pH through proton translocation in response to ATP hydrolysis.[1] Because a number of disease states are pH sensitive, including diabetes, osteoporosis and cancer, the potential of a therapy based on disruption of optimal pH of the disease could be approached by the modulation of V-ATPase activity.[2] A number of V-ATPase inhibitors are known, most of which are natural products,[3] and at least two different binding sites on this multi-domain enzyme have been identified.[4] Palmerolide A (**1**, Scheme 1) is a macrolide from the Antarctic tunicate *Synoicum adareanum*[5] which appears to bind V-ATPases in a similar fashion to bafilomycin A_1 but palmerolide A differs markedly from bafilomycin A_1 in its display of reduced neurological effects in mice. Herein we report additional V-ATPase inhibitors that share palmerolide A's macrolide ring, palmerolides D–G (**2**–**5**, Scheme 1).

2. Results and discussion

2.1. Isolation and structure elucidation

S. adareanum is found commonly in the shallow waters of Antarctica. It is a colonial tunicate that grows as multiple fist-sized colonies emerging from a common base, forming a group of colonies. In the vicinity of Palmer Station, the US field research facility on the Antarctic Peninsula, *S. adareanum* is found in sufficient abundance that a single dive might result in biomass yielding hundreds of milligrams of palmerolides; in fact, the larger individual colony groups themselves may contain up to 100 mg of palmerolide A. However, yields are variable between groups, as is the distribution of more than a dozen different palmerolides isolated to date. Despite the ready availability of palmerolides from the natural source, the harsh and remote location of the *S. adareanum* habitat makes their synthetic[6–8] availability key to further drug developmental studies.

Extracts (1:1 methanol/dichloromethane) from the freeze dried tunicate were fractionated by step gradient chromatography using methanol in ethyl acetate for elution from silica gel. The palmerolides display high chromatographic polarity, with **1**–**5** eluting in 6% methanol in ethyl acetate. Purification is then achieved by HPLC using 40% water in acetonitrile followed by a second HPLC purification step using 20% water in methanol. A typical isolation procedure[9] on 500 g of freeze-dried animal tissue results in a chromatographic sequence of palmerolide E (**3**, 7 mg), F (**4**, 7 mg), A (**1**, 200 mg), G (**5**, 2 mg) and D (**2**, 7 mg), each of which appears as a white or off-white amorphous solid for which crystallization has proved elusive.

Palmerolide D (**2**) exhibited structural features similar to those of palmerolide A (**1**) based on its ^{1}H NMR spectrum (Table 1) but the presence of additional proton signals along with MS analysis indicated an increase in carbon and proton count (HR ESI-MS *m/z* 625.3864, Δmmu 1.1 for $C_{36}H_{53}N_2O_7$). The data from several 2D NMR experiments established the carbon backbone of the macrolide portion of **2** as identical to **1** although some differences were noted in the carboxamide portion of the molecule. For example, (Fig. 1), the C-1 (δ 165.5) to C-3 (δ 149.4) conjugated ester was

* Corresponding author.
E-mail address: bjbaker@usf.edu (B.J. Baker).

0968-0896/$ - see front matter © 2011 Elsevier Ltd. All rights reserved.
doi:10.1016/j.bmc.2011.06.004

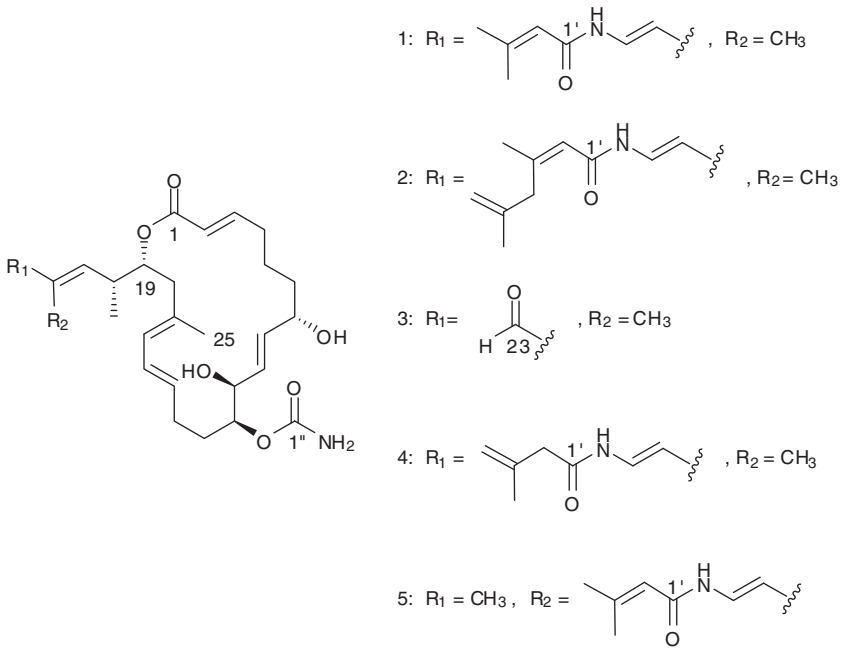

Scheme 1. Palmerolides A (**1**), D (**2**), E (**3**), F (**4**) and G (**5**).

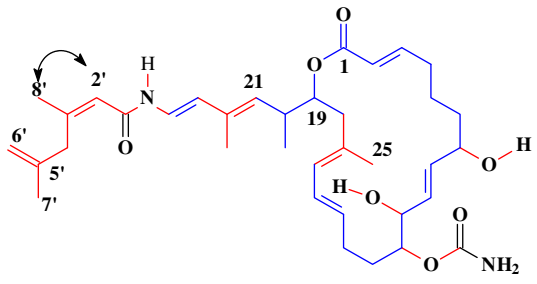

Figure 1. Key palmerolide D (**2**) segments established by gHMBC (red), gCOSY (blue) and ROESY (arrows).

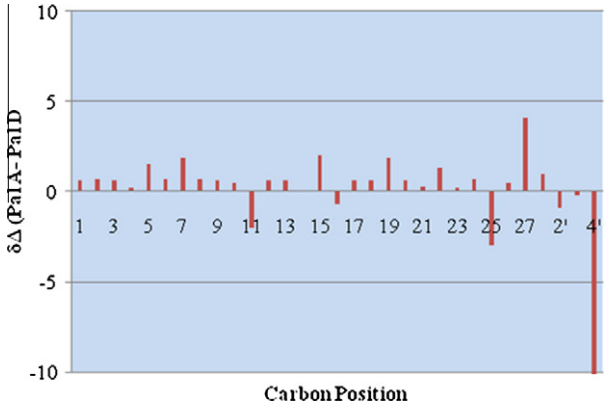

Figure 2. Comparison of palmerolide D and palmerolide A ^{13}C NMR chemical shifts by position number ($\Delta\delta = \delta$ Pal A–δ Pal D)

separated by three methylene groups from the C-7 to C-11 polyfunctionalized substructure. Of the three oxymethines in this region, the mid-field proton, H-10 (δ 4.15), correlated in the gHMBC spectrum to a carbonyl in the ester/amide region of the ^{13}C NMR spectrum (δ 156.8), indicative of the carbamate found on **1**. The C-25 vinyl methyl group was demonstrated to be in position 17 of the C-14 to C-17 diene substructure, one of two such dienes in the molecule. The C-14/C-17 diene was separated by two methylene groups from the C-7/C-11 substructure. As found in palmerolide A, the macrolide was completed by observation of a gHMBC correlation between oxymethine H-19 (δ 4.84) and C-1. C-19 was further correlated to methylene C-18, to a methine, C-20, and to the second diene, C-21/C-24. A doublet methyl, H_3-26 (δ 0.89), could be assigned as the substituent on the C-20 methine while a vinyl methyl, C-27 (δ 12.8), was established on the quaternary C-22 (δ 132.0) olefinic carbon. The *E* geometry of each of the six olefins in the carbon backbone, as found in palmerolide A, was based on $^3J_{H,H}$ (Table 1), NOE, and ^{13}C NMR data. In fact, the ^{13}C NMR spectrum shows no more than a few ppm $\Delta\delta$ when compared to palmerolide A (palmerolide A–palmerolide D) over the contiguous carbon backbone (Fig. 2).

The carboxamide portion of palmerolide D (**2**) was assigned starting from the gHMBC correlation of H-2′ (δ 5.81) to a carbonyl at δ 162.9 (C-1′), a methylene group at δ 40.3 (C-4′), and a methyl group at δ 25.1 (C-8′). These correlations indicated that C-2′ (δ 119.7) was part of a trisubstituted olefin that was conjugated to an amide. The C-2′/C-3′ trisubstituted olefin was assigned as *Z* based on ROESY correlation between H-2′ and H_3-8′. The presence of this conjugated olefin was also supported by gHMBC correlations of H_3-8′ (δ 1.76) to C-2′, C-3′ (δ 152.7), and C-4′. The carboxamide chain could be further elongated based on gHMBC results that indicated H_2-4′ (δ 3.34) correlated to C-2′, C-3′, C-5′ (δ 143.0), and C-7′ (δ 22.0). Further, H_3-7′ (δ 1.61) correlated to C-4′, C-5′, and an olefinic methylene, C-6′ (δ 111.9), completing the planar structure of **2**. The presence of the carbamate functionality on C-11 (δ 75.2) was confirmed by mass spectral data which was consistent with the carbon and hydrogen count established in NMR analysis and a gHMBC correlation from H-11 (δ 4.48) to C-1″ (δ 156.8) carbonyl.

Palmerolide E (**3**) was unusual in displaying a ^1H NMR signal indicative of an aldehyde group (Table 1). Taken with the significantly reduced carbon and proton count established by mass spectral analysis (*m/z* 512.2634 for $C_{27}H_{39}NO_7Na$, calcd 512.2624), but retaining many of the macrolide NMR signals of palmerolide A (**1**),

Table 1
^{1}H and ^{13}C NMR spectral data for palmerolides D (**2**) and E (**3**)[a]

Position		Palmerolide D			Palmerolide E		
		δ_H	δ_C	HMBC	δ_H	δ_C	HMBC
1			165.5			165.2	
2		5.76 (*d*, 15.8)	120.6	1,4	5.77(*d*, 15.7)	120.3	1, 4
3		6.71 (*ddd*, 4, 11.5, 15.7)	149.4	1,2,5	6.74 (*ddd*, 4.3, 11.5, 15.7)	149.7	1, 4,5
4	a	2.14 (*m*)	32.4	2, 3,5	2.15 (*m*)	32.3	2,3,5
	b	2.11 (*m*)			2.00 (*m*)		2,3
5	a	1.31 (*m*)	24.2		1.31 (*m*)	25.0	
	b	1.05 (*m*)			1.07 (*m*)		
6	a	1.51 (*ddd*, 4.4, 7.7, 11.2)	37.8		1.50 (*ddd*, 4.4)	37.8	4,5,7,8
	b	1.33 (*m*)			1.30 (*m*)		5,7,8
7		3.82 (*ddd*, 4.4, 6.5, 7.9)	72.6		3.83 (*ddd*, 4.4, 6.8, 8.2)	72.5	9
8		5.53 (*dd*, 7.9, 15.3)	133.6	7, 9,10	5.54 (*dd*, 8.2, 15.4)	133.6	7,9,10
9		5.49 (*dd*, 2.9, 15.3)	129.0	7,8,11,10	5.49 (*dd*, 2.9, 15.4)	128.9	8,7,10
10		4.15 (*s*)	69.4	11	4.13 (br *s*)	69.2	8,9,11,12/13
11		4.48 (*ddd*, 1.9, 5, 10.6)	75.2	9,10,12,13,1″	4.47 (*ddd*, 1.5, 5.1, 10.7)	75.1	9,10,12/13,1″
12	a	1.60 (*m*)	29.5		1.61	29.4	13
	b	1.01 (*m*)			1.05 (*m*)		13
13		1.94 (*m*)	29.5		1.97 (*m*)	29.4	12,14,15
14		5.41 (*ddd*, 5, 10, 14.6)	132.7	13,16	5.43 (*ddd*, 5.2, 9.8, 14.8)	132.2	12/13,16
15		6.04 (*dd*, 11.6, 14.6)	126.4		6.05 (*dd*, 10.7, 14.8)	126.3	13,14,16
16		5.59 (*d*, 11.6)	127.8	14,15,17,18,25	5.61(*d*, 10.7)	128.0	14,15,17,18,25
17			131.7			131.1	
18	a	2.16 (*dd*, 1.4, 12.8)	43.3	16,17,25	2.16 (*dd*, 1.4, 12.4)	43.0	16,17,25
	b	2.00 (*dd*, 11.9, 12.8)		16,17,19,25	2.07 (*dd*, 11, 12.4)		16,17,19,25
19		4.84 (*ddd*, 1.7, 8.1, 11)	73.9	1,26	5.02 (*ddd*, 2.1, 7.5, 10)	72.6	1,17,20,21,26
20		2.68 (*qdd*, 6.9, 7.7, 9.2)	36.7	19,21	2.64 (*qdd*, 6.8, 7.1, 9.3)	38.1	19,21,22,26
21		5.14 (*d*, 9.7)	130.2	19,26,27	6.55 (*dd*, 1.5, 10.2)	154.9	19,20,23,25,27
22			132.0			138.7	
23		5.86 (*d*, 14.6)	117.0	21,24,27	9.40 (*s*)	195.6	21,22,27
24		6.85 (*dd*, 10.4, 14.6)	122.2	22			
25		1.60 (*s*)	16.3	16,17,18	1.63 (*s*)	16.1	16,17,18
26		0.89 (*d*, 6.7)	17.2	19,20,21	1.01 (*d*, 6.8)	15.5	19,20,21
27		1.70 (*s*)	12.8	21,22,23	1.68 (*s*)	9.2	21,22,23
1′			162.9				
2′		5.81 (*s*)	119.7	1′,4′,8′			
3′			152.7				
4′		3.34(*s*)	40.3	2′,3′,5′			
5′			143.0				
6′		4.72 (*s*)	111.9	4′,7′			
7′		1.61 (*s*)	22.0	4′,5′,6′			
8′		1.76 (*s*)	25.1	2′,3′,4′			
1″			156.8				156.7
1″-NH_2		6.45 (br)			6.48 (br)		
7-OH		4.53 (*d*, 3.8)			4.70 (*d*, 4.1)		
10-OH		5.19 (*m*, 4.5)			5.18 (*d*, 4.9)		
24-NH		9.94 (*d*, 10.3)		1′			

[a] 500 MHz for ^{1}H, 125 MHz for ^{13}C, DMSO-d_6.

3 appeared to be an amide hydrolysis product. Indeed, 2D NMR analysis, including ROESY, found the macrocycle portion to be identical to that of palmerolides **1** and **2**. However, the side chain pendant at C-19 could account for the missing substructures. As found in **1** and **2**, gCOSY and gHMBC spectra established that C-19 was adjacent to a C-20 methine, followed by the familiar C-21/C-22 olefin and its attached vinyl methyl group. In contrast to **1** and **2**, the C-21/C-22 olefin was found to be conjugated to the aforementioned aldehyde function, displaying gHMBC correlations between the aldehyde proton, H-23 (δ 9.40) and both C-21 (δ 154.9) and C-22 (δ 138.7). Thus **3** is not the initially expected hydrolysis product but rather the descarboxamide product.

Palmerolides F (**4**) and G (**5**) were shown by HR ESIMS to be isomeric with **1** (*m/z*: **4**, 607.3359; **5**, 607.3350; calcd 607.3359 for $C_{33}H_{48}N_2O_7Na$). 2D NMR analysis, as described for previous palmerolides, established the carbon backbone, C-1 to C-24, of **4** as identical to **1**, both in constitution as well as olefin geometry (Table 2). For **4** the carboxamide was clearly distinguished as different from **1** by the ^{1}H NMR spectrum and the presence in the ^{13}C NMR spectrum of an olefinic methylene confirmed the observation. In the gHMBC data of **4**, the protons of the olefinic methylene demonstrated correlations to a vinyl methyl group, C-5′ (δ 22.2), and a vinyl methylene, C-2′ (δ 44.5), the latter of which was further correlated to the carboxamide carbonyl, C-1′ (δ 167.4), establishing the carboxamide group as 3-methyl-3-butenoyl. This meant that the only structural difference between **4** and **1** was the isomerization from an internal to a terminal alkene at the end of the carboxamide chain.

The second isomer, palmerolide G (**5**), differed from **1** only in olefin geometry, where the C-21/C-22 configuration was demonstrated as *Z* based on ROESY data showing a correlation between H-23 and H_3-26. The impact of this minor structural difference on the chemical shifts of the surrounding carbons compared to compound **1** can be observed in Figure 3.

2.2. Stereochemical assignment

Stereochemical assignment of the asymmetric centers found in the palmerolides has proven challenging. Palmerolide A (**1**) was originally characterized based strictly on spectral analysis,

Table 2
^{1}H and ^{13}C NMR Spectral Data for Palmerolides F (**4**) and G (**5**)[a]

Position		Palmerolide F			Palmerolide G		
		δ_H	δ_C	HMBC	δ_H	δ_C	HMBC
1			165.3			165.5	
2		5.77 (1H, d, 16.0)	120.5	1,4	5.76 (d, 15.4)	120.5	1,4
3		6.71 (1H, ddd, 4.8, 10.3, 16.0)	149.2	1,2,4,5	6.71 (ddd, 4.8, 10, 15.4)	149.4	1,2,4,5
4	a	2.11 (1H, m)	32.3	2,3,5,6	2.10 (m)	32.6	3,5
	b	1.84 (m)			1.84 (m)		
5	a	1.31 (1H, m)	24.9	6,7	1.28 (m)	25.1	
	b	0.98 (1H, m)		7	1.06 (m)		
6	a	1.48 (1H, m)	37.7	5,7,8	1.49 (ddd,4.4,7.7, 11)	38.6	5,7,8,9
	b	1.30 (1H, m)		5,7,8	1.31		4,7,8
7		3.83(1H, d, 4.0)	72.5	6,9	3.83(ddd, 4.4, 6.5, 7.9)	73.4	
8		5.55 (1H, dd, 7.8, 15.9)	133.5	6,7,9,10	5.54 (dd, 7.9, 14.8)	134.5	7,10
9		5.48 (1H, dd, 2.3, 15.8)	128.8	8	5.46 (dd, 2.2, 14.8)	129.7	7,10
10		4.14 (1H, br s)	69.1	9,12/13	4.13 (s)	70.2	11
11		4.48 (1H dd, 4.6, 11.2)	75.0	9,10,12/13,1″	4.48 (ddd, 1.5, 4.9, 10.8)	76.1	9,10,12,1″
12	a	1.60 (1H, m)	29.3	11,12/13	1.13	30.1	14,15
	b	0.97 (1H, m)		12/13,14	0.98 (m)		
13		1.94 (2H, m)	29.3	12/13,14,15	1.98(m)	30.1	13,15,16
14		5.41 (1H, ddd, 4.2, 10.4, 15.0)	131.9	12/13,16	5.41 (ddd, 4.4,10.1,14.8)	132.9	13,14,16
15		6.05 (1H, dd, 11.2, 15.0)	126.3	16,17,12/13	6.03 (dd, 11.1, 14.8)	127.3	16,18
16		5.59 (1H, d, 10.6)	127.7	14,15,18,25	5.58 (d, 11.1)	128.6	
			131.5			132.5	
17			131.5				
18	a	2.15 (1H, m)	43.2	16,17,25	2.16 (dd, 1.5, 13.2)		
	b	1.99 (1H, q, 12.2)		16,17,19,20,25	1.98 (dd, 12, 13.2)		16,17
19		4.84 (1H, 1.7, 7.9, 12)	73.7	1,17,21,26	4.82 (ddd, 1.5, 8, 12)	74.5	17,18,26
20		2.68 (qdd, 6.7, 7.9, 9.6)	36.5	18,19,21,22,26	2.65 (qdd, 6.6, 8, 10)	40.3	19,21,22,25
21		5.14 (1H, d, 9.6)	130.1	19,20,23,26,27	5.01(d, 10)	129.3	18,23
22			132.3			132.1	
23		5.87 (1H, d, 15.0)	116.9	21,22,24,27	6.19 (d, 14.3)	109.8	21,24
24		6.77 (1H, dd, 10.3, 15.0)	121.8	22,23,1′	6.93 (dd, 10.4,14.3)	125.4	21,22,23
25		1.61 (3H, s)	16.1	16,17,18	1.60 (s)	17.1	14,16
26		0.90 (3H, d, 7.6)	17.0	19,21,20	0.89 (d, 6.6)	18.2	19,20,21
27		1.70 (3H, s)	12.6	21,22,23	1.76 (s)	21.1	21,22,23
1′			167.4			164.1	
2′		2.91 (1H, s)	44.5	1′,3′,4′,5′	5.68	118.7	1′,4′,5′,27
3′			139.8			153.6	
4′	a	4.82 (1H, br s)	113.5	2′,5′	2.12	20.1	1′,2′,3′,5′
	b	4.79 (1H, br s)		2′,3′,5′			
5′		1.71 (3H, s)	22.2	1′,2′,3′,4′	1.84	28.0	2′,3′,4′
7-OH		4.69 (1H, br s)			4.73 (d, 4.4)		
10-OH		5.17 (1H, d, 3.8)		9	5.20 (d, 4.7)		
24-NH		9.93 (1H, d, 10.3)		23,24, 1′	9.97 (d,10.2)		1′
$OCONH_2$		6.48 (2H, br)	156.6		6.48 (s)	157.6	

[a] 500 MHz for ^{1}H, 125 MHz for ^{13}C, DMSO-d_6.

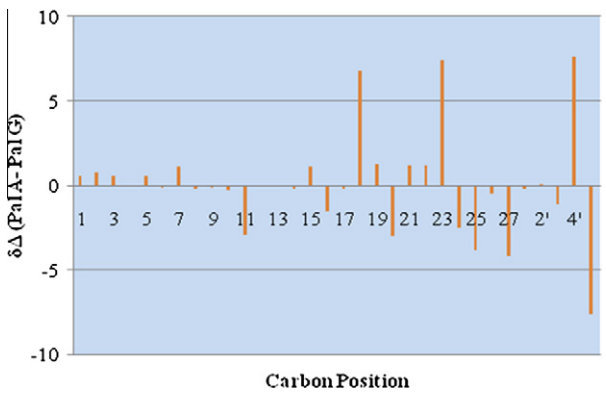

Figure 3. Comparison of palmerolide G and palmerolide A ^{13}C NMR chemical shifts by position number ($\Delta\delta = \delta$ Pal A–δ Pal G)

including NOE, *J*-coupling and chemical shift analysis of diastereomers, but was later revised based on degradative[10] and synthetic studies.[6–8] Assignment of the new palmerolides builds on these previous results. Thus, analysis of palmerolides D-G (**2**–**5**) using Mosher's method[11] demonstrate the C-7 to C-11 substructure of each matches that of palmerolide A (Table 3). Further, conformational analysis based on $^{3}J_{H,H}$ (Table 4) illustrates all four palmerolides share the same conformation at the macrolide linkage. Thus we have the assigned the stereocenters of these new palmerolides as identical to those of palmerolide A (**1**).

2.3. Biological evaluation

Palmerolide A (**1**) was reported to be a potent inhibitor of the ATP-driven proton translocation activity of V-pump by blocking its V_0 proton channel, similar to the inhibitory mechanism of bafilomycin A_1[12] and salicylihalamide A.[4,13] As expected based on this observation, palmerolide A does not inhibit the ATP hydrolysis activity of the isolated V_1 sector. Interestingly, some preparations of palmerolide A appear to stimulate the Ca-ATPase activity of the intact V-ATPase holoenzyme, suggesting that it may facilitate the dissociation between V_1 and V_0 domains. However, this activity of palmerolide A did not correlate well with other preparations of the same compound and therefore may be attributed to minor components in palmerolide preparations which are not yet identified.

Table 3
Stereochemical analysis ($\Delta\delta$) of palmerolides A-F (**1**–**5**) using Mosher's method

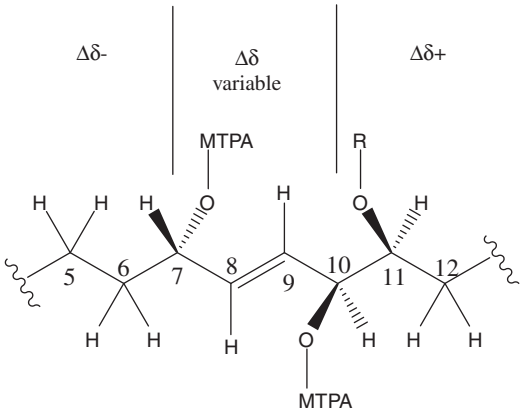

	Pal A (**1**)	Pal D (**2**)	Pal E (**3**)	Pal F (**4**)	Pal G (**5**)
H-5a	—	−0.01	−0.01	−0.02	—
H-5b	−0.15	—	—	—	−0.13
H-6a	−0.02	−0.03	−0.03	−0.04	−0.03
H-11	+0.11	+0.13	+0.14	+0.09	+0.14
H-12	+0.18	+0.17	+0.15	+0.13	+0.12

Table 4
$^{3}J_{H,H}$ coupling constants (Hz) established by NMR simulation

Proton	Pal A (**1**)	Pal D (**2**)	Pal E (**3**)	Pal F (**4**)	Pal G (**5**)
H-19–H-20	10.0	10.0	9.9	9.7	10.0
H-20–H-21	8.0	8.0	7.0	7.3	8.0
H-20–H_3-26	6.6	6.6	6.9	7.0	6.6

Table 5
Bioactivity data for palmerolides (IC_{50} values in μM)

Compound	V-ATPase (μM)	Melanoma (μM)	v-ATPase: cytotoxicity ratio
	Mammalian	UACC-62	
Palmerolide A (**1**)	0.002	0.024*	0.083
Palmerolide D (**2**)	0.025	0.002	12.5
Palmerolide E (**3**)	>10.000	5.000	>2
Palmerolide F (**4**)	0.063	0.758	0.083
Palmerolide G (**5**)	0.007	1.207	0.006

* LC_{50} = 0.018 μM reported in 2006 from NCI 60 cell line panel results.[5]

The new palmerolides have been evaluated for cytotoxicity against UACC-62 melanoma cells as well as their ability to inhibit V-ATPase (Table 5). The primary trend apparent in these bioactivity data sets is that the carboxamide structure has only minimal influence on the cytotoxic activity but is required for V-ATPase inhibition. Palmerolide E, lacking the entire carboxamide functionality, appears to retain inhibitory activity (IC_{50} 5 μM) toward melanoma while losing effectiveness against V-ATPase (IC_{50} >10 μM). Conversely, palmerolide D which possess the extended side chain demonstrates a 10-fold decrease in V-ATPase inhibitory activity in comparison to palmerolide A, but shows a 10-fold increase in cytotoxicity against melanoma. A similar observation was made by Nicolaou et al. in their biological evaluation of chemically synthesized palmerolide A analogues.[14] A marked increase in cytotoxic activity was noted upon addition of a non-polar aromatic system to the side chain enamide.

These data sets also suggest that the C-2′/C-3′ trisubstituted alkene may have some influence on V-ATPase inhibition but does not appear to influence the cytotoxicity of the palmerolides. Interestingly, palmerolides A (0.002 μM), D (0.025 μM), and G (0.007 μM), all of which contain the C-2′/C-3′ olefin are very potent V-ATPase inhibitors whereas palmerolide F which lacks the abovementioned olefin (0.063 μM) is significantly less potent. It is also of note that the isomerization of the C-21/C-22 trisubstituted olefin from the *E*-geometry to *Z* significantly affects the cytotoxicity of palmerolide G while barely affecting V-ATPase inhibiting ability. This data not only suggests that substructures within the side chain influence the overall bioactivity but also implies that different parts of the side chain are responsible for the activities exhibited against UACC-62 and V-ATPase.

Palmerolides are less neurotoxic than other V-ATPase inhibitors (unpublished data), which leads us to believe that they bind more than one cellular target. In an effort to help prove or disprove this theory the bioactivity ratios for the palmerolides were calculated and shown in Table 5. It was anticipated that if some of the palmerolides lost considerable V-ATPase inhibiting activity while gaining significant cytotoxicity, particularly relative to palmerolide A, then the polymodal mechanism of action would be apparent in the ratios. If this were the case then a reciprocal ratio to that of palmerolide A would be expected. Though the data is preliminary and still inconclusive, the closest example of this was found in palmerolide D. Additional SAR studies could provide more insight into the presumed polymodal mechanism of cytotoxicity in the palmerolides as well as continue to reveal important correlations between their structures and bioactivity.

3. Experimental

3.1. General experimental procedures

Optical rotations were measured on a Rudolph Research Analytical AUTOPOL® IV digital polarimeter. IR and UV spectra were measured on a Nicolete Avatar 320FT infrared and a Hewlett-Packard 8452A diode array spectrophotometer, respectively. NMR spectra were recorded on a Varian Inova 500 MHz spectrometer. Chemical shifts are given as δ (ppm) with TMS as internal standard. The low resonance mass spectra were recorded on an Agilent Technologies LC/MSD VL electrospray ionization mass spectrometer. The high resonance mass spectra were recorded on an Agilent Technologies LC/MSD TOF electrospray ionization spectrometer. Flash column chromatography was carried out on EM Science silica gel 60 of 230–400 mesh. High performance liquid chromatography was carried out on preparative YMC-Pack ODS-AQ reverse phase columns (250 × 20 mm) and analytical columns (250 × 10 mm) using an LC-8A Shimadzu multi-solvent delivery system, an SCL-10A Shimadzu system controller, and an SPD-10A Shimadzu UV–Vis detector. The purity of all compounds tested was established as ⩾95% via high performance liquid chromatography.

3.2. Biological material

The tunicate *S. adareanum* was collected by hand using SCUBA near Palmer Station on the Antarctic Peninsula between 2000 and 2007. The specimens were immediately frozen and kept frozen until extraction. Only specimens from the same collection season were pooled and 0.5–1.5 kg extracted at a time. A voucher specimen was identified by Dr. Linda Cole at the Smithsonian Institution, Washington, D.C.

3.3. Natural product extraction and isolation

Freeze dried *S. adareanum* was extracted with CH_2Cl_2/MeOH. The extract was concentrated and the residue was partitioned between EtOAc and H_2O. Subsequently, the EtOAc layer was dried with $MgSO_4$ and concentrated in vacuo. The crude organic extract was subjected to flash column chromatography with an EtOAc/MeOH solvent system to give 10 fractions. These fractions were further separated using 40% H_2O/MeCN, and the fractions obtained from the separation were subsequently purified using 20–30% H_2O/MeOH to afford pure palmerolides A (**1**), D (**2**), E (**3**), F (**4**), and G (**5**).

3.4. Palmerolide D (2)

Colorless solid; $[\alpha]_D^{25}$ +67 (*c* 0.5, MeOH); UV/Vis (MeOH) λ_{max} (ε): 216 (1742), 248 (528); IR (thin film): 3327, 2939, 2829, 2061, 1716, 1558. 1455, 1261, 1025, 975 cm^{-1}; LR ESIMS (+) *m/z* 625.6, HR ESIMS (+) *m/z* 625.3864 ($C_{36}H_{53}N_2O_7$ requires 625.3853); ^1H and ^{13}C NMR, see Table 1.

3.5. Palmerolide E (3)

Colorless solid; $[\alpha]_D^{25}$ +17 (*c* 0.1, MeOH); UV/Vis (MeOH) λ_{max} (ε): 216 (1295), 248 (645); IR (thin film): 3635, 2940, 2830,1715, 1637, 1540, 1387, 1276, 1194, 1079, 938 cm^{-1}; LR ESIMS (+) *m/z* 601.5, HR ESIMS (+) *m/z* 512.2634 ($C_{27}H_{39}NO_7$ Na requires 512.2624); ^1H and ^{13}C NMR, see Table 1.

3.6. Palmerolide F (4)

Yellow solid; $[\alpha]_D^{22}$ −67.1 (*c* 0.5, MeOH); UV/Vis (MeOH) λ_{max} (ε): 213 (413), 262 (229); IR (thin film): 3340, 3013, 1705, 1642, 1524, 1318, 1216, 1187, 1018, 976 cm^{-1}; LR ESIMS (+) *m/z* 607 $[M + Na]^+$; HR ESIMS (+) *m/z* 607.3359 ($C_{33}H_{48}N_2O_7Na$ requires 607.3359); ^1H and ^{13}C NMR data, see Table 2.

3.7. Palmerolide G (5)

Yellow solid; $[\alpha]_D^{22}$ −27.1 (*c* 0.1, MeOH); UV/Vis (MeOH) λ_{max} (ε) = 216 (719),262 (403); IR (thin film): 3383, 2927, 1705, 1638, 1522, 1457, 1377, 1279, 1216, 1194, 1024 cm^{-1}; HR ESIMS $[M + Na]^+$ *m/z* 607.3350 ($C_{33}H_{48}N_2O_7Na$ requires 607.3359); ^1H and ^{13}C NMR data, see Table 2.

3.8. Preparation and reconstitution of V-pump and V_0 proton channel

The bovine brain V-pump and the dissociated V_0 sector, prepared as described previously,[13,14] were reconstituted into proteoliposomes, which contain phosphatidylcholine (PC), phosphatidylethanolamine (PE), phosphatidylserine (PS) and cholesterol at a weight ratio of 40:26.5:7.5:26, by the cholate dilution, freeze-thaw method, as described.[4,13] In brief, liposomes (200 μg) were mixed with either 1 μg of V-ATPase or 0.5 μg of V_0 sector, followed by addition of glycerol, Na-cholate, KCl, and $MgCl_2$ to final concentrations of 10% (vol/vol), 1%, 0.15 M and 2.5 mM, respectively. The reconstitution mixtures were then incubated at room temperature (rt) for 1 h, frozen in liquid N_2 and thawed at rt. For ATPase and proton pumping assays, the mixture was directly diluted with 0.2 ml of ATPase assay solution in a test tube or 1.5 ml of the proton pumping assay buffer in a spectrophotometer cuvette, respectively, which allows for the formation of sealed and ready-to-assay proteoliposomes. For proton channel assays, the reconstitution mixture was first diluted 50-fold in dilution buffer (150 mM KCl, 20 mM Na–Tricine, pH 7.5 and 3 mM $MgCl_2$), and centrifuged to precipitate the sealed proteoliposomes. The sealed proteoliposomes were then suspended in a small volume of the dilution buffer.

3.9. Measurement of ATP-driven proton translocation

Both assays for ATP-driven proton translocation and for proton channel activity were conducted in a SLM-Aminco DW2C dual wavelength spectrophotometer and the activity was registered as $\Delta A_{492-540}$. For ATP-driven proton pumping assay, 5–10 μl proteoliposomes were added to 1.5 ml of assay buffer containing 20 mM Tricine, pH 7.0, 6.7 μM acridine orange, 3 mM $MgCl_2$, and 150 mM KCl. The reaction was initiated by addition of 1.3 mM ATP (pH 7.0) and 1 μg ml^{-1} valinomycin, and was terminated by addition of the proton ionophore 1799.

3.10. Measurement of proton channel activity

The proton channel activity of V_0 sector was performed as described.[15] In brief, the reconstituted proteoliposomes of V_0, sealed with 150 mM KCl inside as described above, were activated by incubating with 2 μl of 0.5 M MES (pH 3.4) per 5 μl of the proteoliposomes for 30 min at room temperature prior to assay. The membrane potential-driven proton translocation assay was also conducted in a SLM-Aminco DW2C dual wavelength spectrophotometer and the activity was registered as $\Delta A_{492-540}$. The assay solution contained 150 mM NaCl, 30 mM Tricine, pH 7.5, 3 mM $MgCl_2$, and 6 μM acridine orange. The reaction was initiated by addition of 1 μM of valinomycin and finished by addition of 1799.

3.11. Cytotoxicity assay

All tissue culture components were purchased from Fisher Scientific. The UACC-62 human melanoma cell line was provided by the National Cancer Institute (NCI), Division of Cancer Treatment and Diagnosis (DCTD). The cancer cells were cultured in RPMI supplemented with 10% fetal bovine serum, 2 mM glutamine, and 50 μg ml^{-1} gentamicin. The cytotoxicity of the compounds was determined using the sulphorhodamine B (SRB) assay. A 96-well plate was inoculated with 100 μl of cell suspension in each well at a plating density of 5000 cells/well. The plate was incubated at 37 °C with 5% CO_2, 95% air and 100% relative humidity for 24 h prior to addition of experimental drugs. After the cells attach to the bottom of the plate in the 24 h period, 100 μl of medium containing five different drug concentrations (10, 1, 0.1, 0.01, 0.001 μM) of the compounds to be tested were added to the respective wells in triplicate. The assay plate was incubated for 48 h following drug addition at 37 °C with 5% CO_2, 95% air and 100% relative humidity. The plate was removed from the incubator and the media aspirated from the wells. The cells were fixed using 50 μl of 10% cold trichloroacetic acid and kept at 4 °C for 1 h, subsequently being washed five times with distilled water. The plates were air-dried at rt and the cells stained with 100 μl of SRB solution (0.4% w/v SRB in 1% v/v acetic acid) for 10 min. The plate was washed five times with 1% acetic acid to remove excess SRB present in the wells and allowed to air dry. Protein bound stain was solubilized with 200 μl of tris base and mixed. The absorbance was measured at 515 nm using a BioTek Synergy 2 microtitre plate reader and the IC_{50} values determined by plotting the optical density of SRB against the drug concentration for each well using the program Table Curve 2D v5.01.

Acknowledgments

We thank Dan Martin, Craig Asmack, Alan Maschek, Philip Bucolo, Matt Lebar, Kevin Peters, Maggie Amsler, Drs. Katrin Iken and Anne Fairhead for field assistance, Edwin Rivera for NMR advice, the NCI for bioassays, and staff of Raytheon Polar Services

and NSF's United States Antarctic Program for logistical support. This research was funded by the NSF (OPP-0125181 and -0442769 to C.D.A. and J.B.M., OPP-0125152, -0296207 and -0442857 to B.J.B.)

Supplementary data

Supplementary data associated with this article can be found, in the online version, at doi:10.1016/j.bmc.2011.06.004.

References and notes

1. Nishi, T.; Forgac, M. *Nature Rev. Mol. Cell Biol.* **2002**, *3*, 94.
2. Forgac, M. *Nature Rev. Mol. Cell Biol.* **2007**, *8*, 917.
3. Beutler, J. A.; McKee, T. C. *Curr. Med. Chem.* **2003**, *10*, 787.
4. Xie, X. S.; Padron, D.; Liao, X.; Wang, J.; Roth, M. G.; De Brabander, J. K. *J. Biol. Chem.* **2004**, *279*, 19755.
5. Diyabalanage, T.; Amsler, C. D.; McClintock, J. B.; Baker, B. J. *J. Am. Chem. Soc.* **2006**, *128*, 5630.
6. Jiang, X.; Liu, B.; Lebreton, S.; De Brabander, J. K. *J. Am. Chem. Soc.* **2007**, *129*, 6386.
7. Nicolaou, K. C.; Guduru, R.; Sun, Y.-P.; Banerji, B.; Chen, D. Y.-K. *Angew. Chem., Int. Ed.* **2007**, *46*, 5896.
8. Nicolaou, K. C.; Sun, Y. P.; Guduru, R.; Banerji, B.; Chen, D. Y. *J. Am. Chem. Soc.* **2008**, *130*, 3633.
9. Diyabalanage, T. Dissertation, University of South Florida, Tampa, 2006.
10. Lebar, M.; Baker, B. J. *Tetrahedron Lett.* **2007**, *48*, 8009.
11. Ohtani, I.; Kusumi, T.; Kashman, Y.; Kakisawa, H. *J. Am. Chem. Soc.* **1991**, *113*, 4092.
12. Bowman, E. J.; Siebers, A.; Karlheinz, A. *Proc. Natl. Acad. Sci. U.S.A.* **1988**, *85*, 7972.
13. Boyd, M. R.; Farina, C.; Belfiore, P.; Gagliardi, S.; Kim, J. W.; Hayakawa, Y.; Beutler, J. A.; McKee, T. C.; Bowman, B. J.; Bowman, E. J. *J. Pharmacol. Exp. Ther.* **2001**, *297*, 114.
14. Nicolaou, K. C.; Leung, G. Y. C.; Dethe, D. H.; Guduru, R.; Sun, Y.-P.; Lim, C. S.; Chen, D. Y.-K. *J. Am. Chem. Soc.* **2008**, *130*, 10019.
15. Goering, B. K. Ph.D. Dissertation, Cornell University, 1995.